

Article

Ppb-Level Hydrogen Sulfide Gas Sensor Based on the Nanocomposite of MoS₂ Octahedron/ZnO-Zn₂SnO₄ Nanoparticles

Di Wu and Ali Akhtar *

School of Information Science and Technology, Dalian Maritime University, Dalian 116026, China

* Correspondence: dr.ali409@dlnu.edu.cn; Tel.: +86-177-0982-1657

Abstract: Hydrogen sulfide (H₂S) detection is extremely necessary due to its hazardous nature. Thus, the design of novel sensors to detect H₂S gas at low temperatures is highly desirable. In this study, a series of nanocomposites based on MoS₂ octahedrons and ZnO-Zn₂SnO₄ nanoparticles were synthesized through the hydrothermal method. Various characterizations such as X-ray diffraction (XRD), Brunauer–Emmett–Teller (BET), scanning electron microscopy (SEM), transmission electron microscopy (TEM), energy-dispersive X-ray spectroscopy (EDS) and X-ray photoelectron spectrum (XPS) have been used to verify the crystal phase, morphology and composition of synthesized nanocomposites. Three gas sensors based on the nanocomposites of pure ZnO-Zn₂SnO₄ (MS-ZNO-0), 5 wt% MoS₂-ZnO-Zn₂SnO₄ (MS-ZNO-5) and 10 wt% MoS₂-ZnO-Zn₂SnO₄ (MS-ZNO-10) were fabricated to check the gas sensing properties of various volatile organic compounds (VOCs). It showed that the gas sensor of (MS-ZNO-5) displayed the highest response of 4 to 2 ppm H₂S and fewer responses to all other tested gases at 30 °C. The sensor of MS-ZNO-5 also displayed humble selectivity (1.6), good stability (35 days), promising reproducibility (5 cycles), rapid response/recovery times (10 s/6 s), a limit of detection (LOD) of 0.05 ppm H₂S (R_a/R_g = 1.8) and an almost linear relationship between H₂S concentration and response. Several elements such as the structure of MoS₂, higher BET-specific surface area, n-n junction and improvement in oxygen species corresponded to improving response.

Keywords: ZnO-Zn₂SnO₄ nanoparticles; MoS₂ octahedron; hydrothermal method; n-n junction; gas sensor; H₂S



Citation: Wu, D.; Akhtar, A.

Ppb-Level Hydrogen Sulfide Gas Sensor Based on the Nanocomposite of MoS₂ Octahedron/ZnO-Zn₂SnO₄ Nanoparticles. *Molecules* **2023**, *28*, 3230. <https://doi.org/10.3390/molecules28073230>

Academic Editor: Eugenio Aprea

Received: 8 February 2023

Revised: 24 March 2023

Accepted: 28 March 2023

Published: 4 April 2023



Copyright: © 2023 by the authors. Licensee MDPI, Basel, Switzerland. This article is an open access article distributed under the terms and conditions of the Creative Commons Attribution (CC BY) license (<https://creativecommons.org/licenses/by/4.0/>).

1. Introduction

H₂S gas, which has a rotten egg smell, could be considered one of the hazardous gases [1] which has an atrocious influence on human health. The long-term exposure to H₂S gas at low concentrations (25–50 ppm) causes various diseases such as headaches, dizziness, nausea, vomiting and irritation in the eyes, etc. Moreover, high concentrations of H₂S (more than 120 ppm) exposure may result in acute poisoning, paralysis and even sometimes death [2,3]. Thus, the veracious and real-time detection of H₂S gas at low temperatures is very decisive, which is enabled by various semiconductor metal oxide (SMO)-based gas sensors.

Several gas sensors based on SMOs such as zinc oxide (ZnO), zinc gallate (ZnGa₂O₄), tin oxide (SnO₂), nickel cobaltite (NiCo₂O₄), zinc stannate (Zn₂SnO₄), copper oxide (CuO), etc., possess some good properties such as precision, low cost, small dimensions, long-term stability and environmental friendliness; because of these properties, SMOs could be considered the primary candidates for the detection of toxic gases as well in photo-catalysis, etc. [4–10]. Plenty of research has shown that some complex metal oxides have been widely used as gas sensors in the last decades. Among these SMOs, an n-type SMOs Zn₂SnO₄ is an imperative ternary metal oxide with some properties such as high chemical stability and electron mobility, high conductivity, low visible adsorption, etc., have been studied widely in various fields such as photo-catalysis, solar cells and gas sensors [11–13]. Furthermore,

ZnO, an n-type semiconductor material, has also been studied in various fields. The study described by An et al. showed that the sensor based on Zn_2SnO_4 detected the highest response to ethanol when compared with H_2 [14]. Additionally, during the study on the sensing properties of ZnO nanosheets and nanorods, it was revealed that the sensor of ZnO nanosheets detected 100 ppm ethanol; by making comparison, it was noted that the response of nanosheets was 4.7-fold that of nanorods [15]. Some other sensors, such as Zn_2SnO_4 -/ZnO-loaded Pd-based sensors, enhanced H_2 sensing properties; the sensors based on the ZnO– SnO_2 – Zn_2SnO_4 hetero-junction, Pt– Zn_2SnO_4 hollow octahedron and Zn_2SnO_4 /ZnO, revealed better gas sensing performances towards ethanol, acetone and formaldehyde, respectively [16–18]. However, pure metal oxides still face some demerits such as low response, high operating temperature, poor selectivity, etc. Therefore, their coupling with 2D materials is essential to increase the gas sensing properties of SMO-based gas sensors.

In the last few years, another research approach based on the emergence of 2D materials into SMOs has received great attention in various fields. Due to some rare properties such as narrow band gap, low density and thermal constancy, these have gained significant attention in the field of photo-catalysis, gas sensing, etc. [19–24]. Typical among transition metal dichalcogenides (TMDs), MoS_2 has received great attention as a fascinating candidate. This is not only as a gas sensor, but MoS_2 can also be used for potential applications in the fields of photodetectors, solar cells, etc. [25–27]. Consequently, the synthesis of 2D material MoS_2 is essential, which would accelerate the adsorption of oxygen molecules as well as increase gas sensing properties. For instance, various 2D materials and metal oxide-based gas sensors such as MoS_2 -reduced graphene oxide nanohybrid, MoS_2 @ MoO_3 magnetic hetero-structure, wool-based carbon fiber/ MoS_2 composite and ZnO– MoS_2 nanocomposites were used to detect various types of VOCs, accompanied by high response, good selectivity, rapid response/recovery times, etc. [28–31].

The purpose of the current study was the detection of hazardous gases. In this regard, a series of gas sensors based on pure ZnO– Zn_2SnO_4 nanoparticles and octahedron MoS_2 were synthesized via a simple hydrothermal method. To date, no literature has been reported on low-temperature gas sensors, such as 30 °C H_2S gas sensors based on a MoS_2 -ZnO– Zn_2SnO_4 nanocomposite. Three gas sensors based on various nanocomposites (MS-ZNO-0, MS-ZNO-5, MS-ZNO-10) were tested to detect different hazardous gases, and our results studied that the highest response of 4 to 2 ppm H_2S was received by the gas sensor of MS-ZNO-5. Furthermore, it revealed humble selectivity, good stability, rapid response/recovery times and LOD, promising reproducibility and an almost linear relationship between H_2S concentration and response, suggesting its potential applicability in the field of gas sensors. Hence, the decoration of ZnO– Zn_2SnO_4 nanoparticles with octahedron MoS_2 is expected to enable the generation of a novel sensor for H_2S sensing.

2. Results and Discussion

2.1. Characterizations of Materials

Figure 1a showed the XRD diffraction peaks of synthesized nanocomposites MS-ZNO-0, MS-ZNO-5 and MS-ZNO-10. The PDF numbers of Zn_2SnO_4 , ZnO and MoS_2 were PDF#24-1470, PDF#36-1451 and PDF#50-0739, respectively. Two diffraction peaks, cited at 2θ values of 34.42° and 36.25° , were matched well to the (002) and (101) crystal planes of ZnO. Furthermore, various peaks of Zn_2SnO_4 were found at 17.72° , 34.29° , 41.68° , 55.11° and 60.44° , and corresponded to the (111), (311), (400), (511) and (440) crystal planes of Zn_2SnO_4 , respectively. The peak observed at half maximum (β) of the (311) and (002) was studied to check the average crystallite sizes. It was also notable that very fine peaks of MoS_2 were also cited in both the nanocomposites (MS-ZNO-5 and MS-ZNO-10) at the 2θ values of 14.37 and 29.09, signified to the (002) and (004) crystal planes of MoS_2 . The estimated mean crystallite sizes such as 10.5, 22.5 and 12 of ZnO– Zn_2SnO_4 were examined by the Scherrer formula [32] in MS-ZNO-0, MS-ZNO-5 and MS-ZNO-10, respectively. The addition of MoS_2 was reasoned to augment the crystallite sizes in both nanocomposites.

Besides, the presence of MoS₂ in composites was confirmed by other characteristics as well, such as SEM, TEM, EDS, XPS, etc. In order to check the BET-specific surface areas of three samples, N₂ adsorption–desorption isotherms were studied in Figure 1b. The BET surface areas of MS-ZNO-0, MS-ZNO-5 and MS-ZNO-10 were 3.46, 20.15 and 13.16 m²/g, respectively. In addition, Figure 1c showed that the average pore sizes of MS-ZNO-0, MS-ZNO-5 and MS-ZNO-10 were 11.1 nm, 8.1 nm and 11.3 nm, respectively.

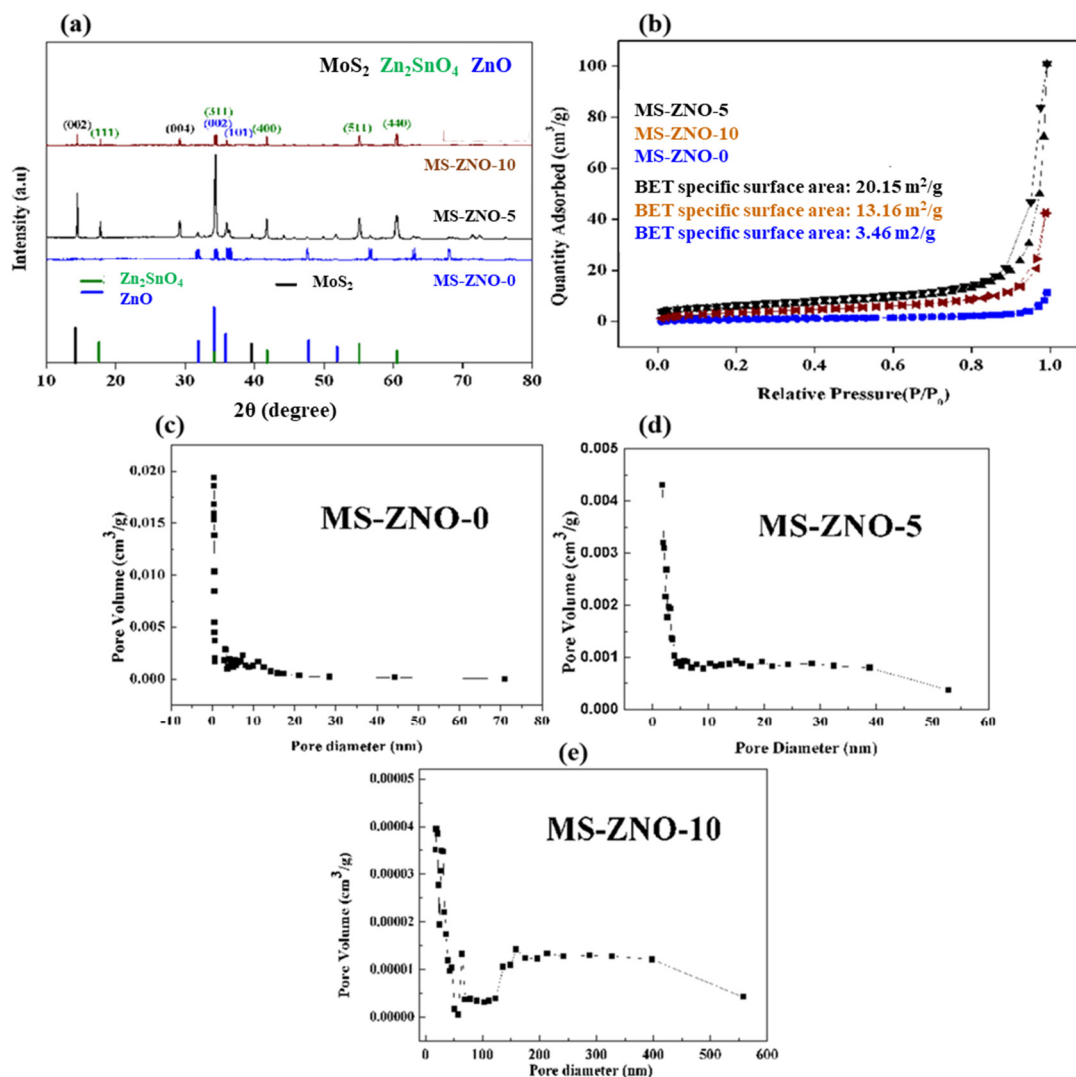


Figure 1. (a) XRD patterns; (b) N₂ adsorption–desorption isotherms; (c) pore size distribution of MS-ZNO-0; (d) pore size distribution of MS-ZNO-5; (e) pore size distribution of MS-ZNO-10.

As shown in Figure 2a–f, the morphology of the synthesized nanocomposites was observed from the SEM graphs. In Figure 2a,b, the SEM graphs of MS-ZNO-0 have been described. The ZnO-Zn₂SnO₄ nanoparticles, with an average particle size of 200–250 nm, were evaluated from the SEM images, while their modification with octahedron MoS₂ was also confirmed from the SEM graphs of MS-ZNO-5 and MS-ZNO-10 in Figure 2c,d and Figure 2e,f, respectively. The SEM and TEM results showed that the relative particle sizes of ZnO-Zn₂SnO₄ nanoparticles and octahedron MoS₂ were increased by the addition of MoS₂ contents in the nanocomposite of MS-ZNO-5 but decreased a little in the nanocomposite of MS-ZNO-10, which also corresponds to the XRD results.

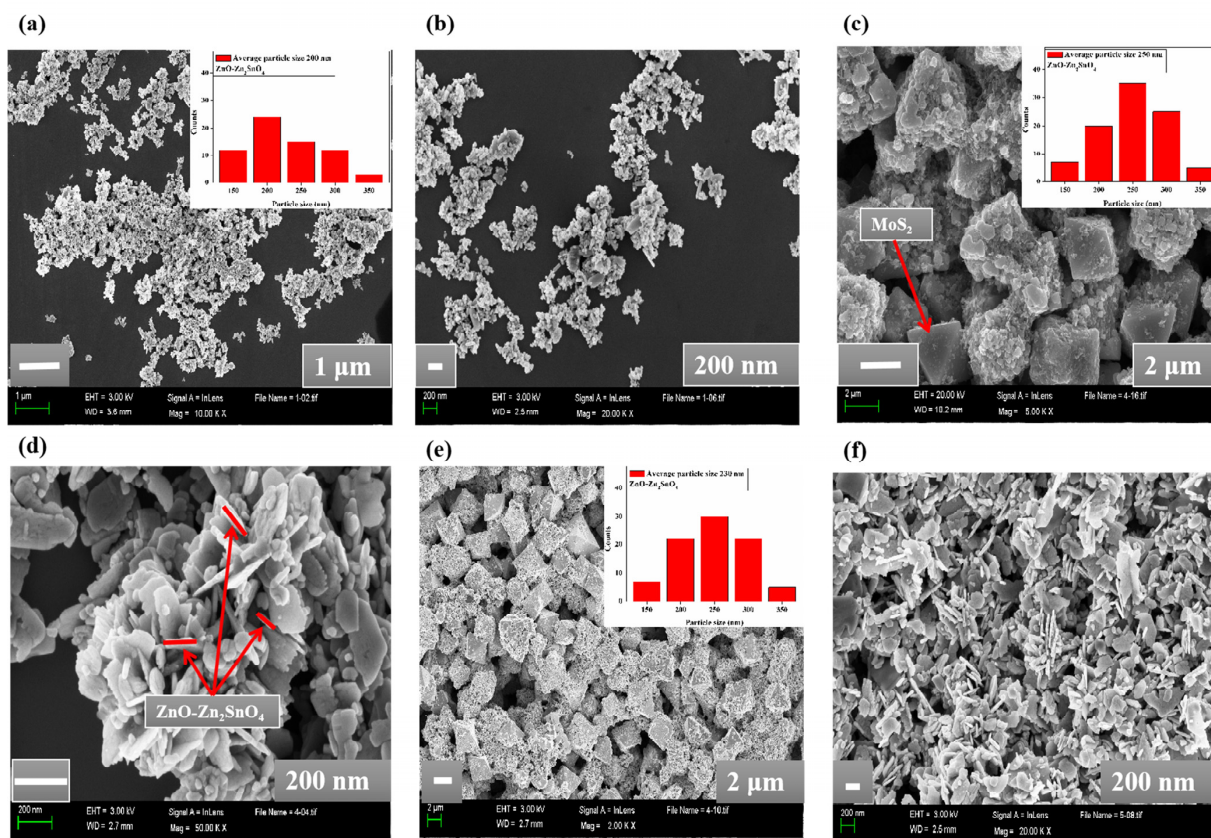


Figure 2. Morphologies of the nanocomposites: (a,b) SEM images of MS-ZNO-0; (c,d) SEM images of MS-ZNO-5; (e,f) SEM images of MS-ZNO-10.

In Figure 3a–f, TEM results also proved the existence of MoS_2 in nanocomposites of MS-ZNO-5 and MS-ZNO-10, with average particle sizes of 200–250 nm for $\text{ZnO-Zn}_2\text{SnO}_4$ nanoparticles in the nanocomposites, as shown below. The TEM graphs of MS-ZNO-5 in Figure 3a–f stated that particle size of $\text{ZnO-Zn}_2\text{SnO}_4$ nanoparticles was enhanced, while the size of octahedron MoS_2 was almost $3.2 \mu\text{m}$ and $2.3 \mu\text{m}$ in the TEM graphs of MS-ZNO-5 and MS-ZNO-10, respectively. The presence of octahedron MoS_2 was further proved from the EDS spectrum of MS-ZNO-5. In Figure 3g, the EDS mapping images of Zn, Sn, O, Mo and S stated that each element had a uniform scattering effect in the nanocomposite of MS-ZNO-5.

The XPS data were fitted by XPSPEAK41 software. The X-ray photo-electron spectroscopy (XPS) results were revealed in Figure 4. The full XPS spectrum of the MS-ZNO-5 composite was disclosed in Figure 4a, which revealed the presence of all the elements such as Zn, Sn, O, Mo and S. In the XPS spectrum of Zn 2p (Figure 4b), two peaks, positioned at 1020.7 and 1043.8 eV, corresponded to Zn $2p_{3/2}$ and Zn $2p_{1/2}$ [33]. These results pointed out that Zn ions in the composite have a valence state of “+2”. In Figure 4c, the Sn 3d spectrum showed two peaks appearing at 485.6 and 496.1 eV corresponding to Sn $3d_{5/2}$ and Sn $3d_{3/2}$, respectively [34]. Additionally, one satellite peak at the value of 497.1 eV was cited. The O 1s spectrum of MS-ZNO-5 demonstrated more oxygen adsorption sites (O_V), which was one of the factors required to enhance the gas sensing properties [8]. The peaks at the values of 529.5 and 530.8 eV in Figure 4d were matched to a typical metal–oxygen bond and defect sites in the XPS spectrum of MS-ZNO-5; on the contrary, in the XPS spectrum of MS-ZNO-0, the two peaks were cited at the values of 529.4 and 530.8 [35,36]. In the high-resolution spectra of Mo 3d, four peaks were cited. The peaks at the values of 225.1, 227.9, 231.1, 234.4 and 283.8 eV, shown in Figure 4e, were related to S 2s, $\text{Mo}^{4+} 3d_{5/2}$, $\text{Mo}^{4+} 3d_{3/2}$, and $\text{Mo}^{6+} 3d_{5/2}$, respectively [37]. In Figure 4f, the peaks at the values of 160.8 eV and 162.0 eV were related to S $2p_{3/2}$ and S $2p_{1/2}$, respectively, in MoS_2 [37].

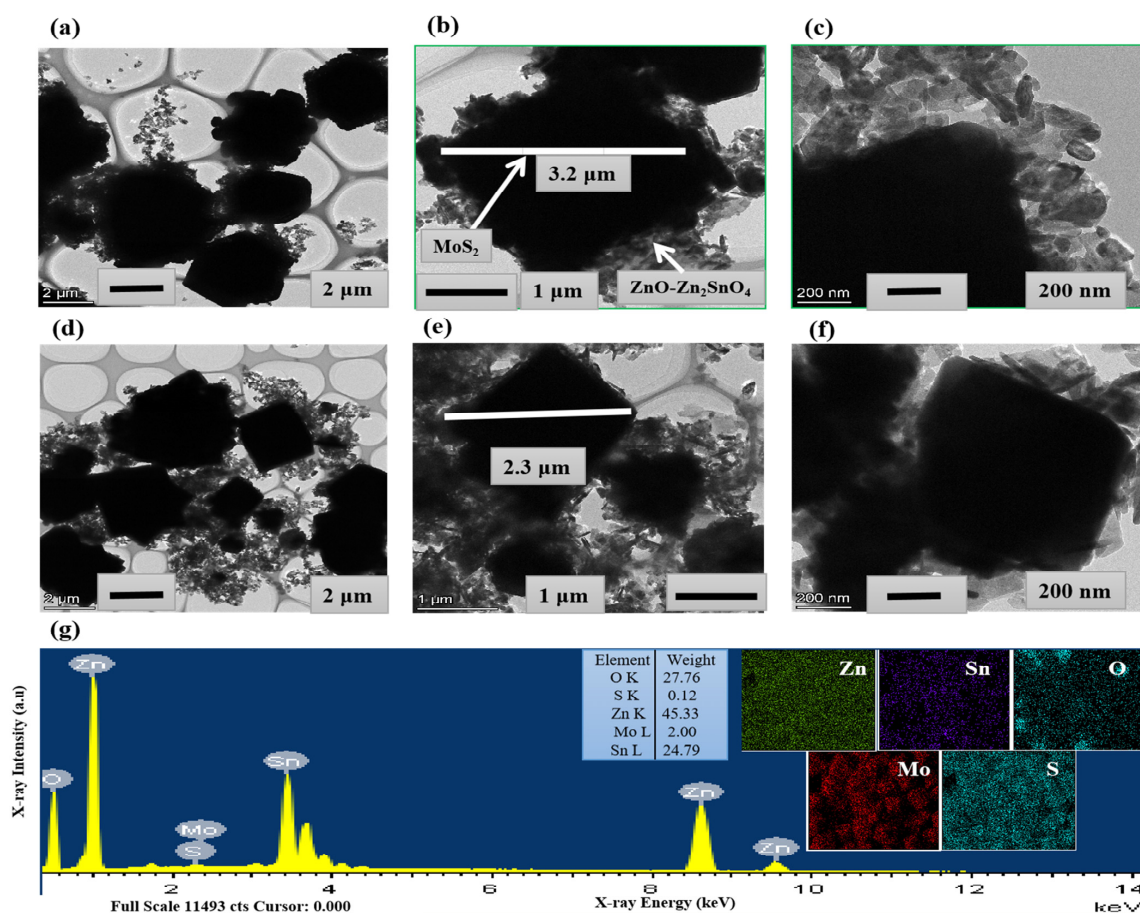


Figure 3. (a–c) TEM images of MS-ZNO-5; (d–f) TEM images of MS-ZNO-10; (g) EDS mapping and spectrum of all elements in MS-ZNO-5.

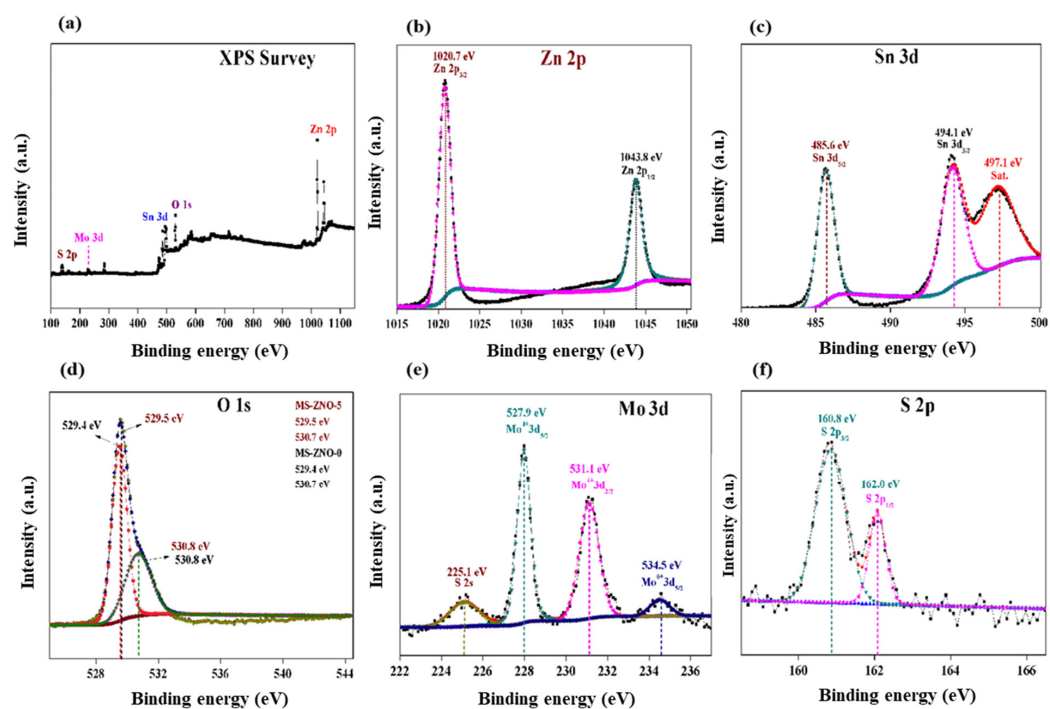


Figure 4. (a) XPS survey of MS-ZNO-5; (b,c) Zn 2p and Sn 3d spectrum's of MS-ZNO-5; (d) O 1s spectrum of MS-ZNO-5 and MS-ZNO-0; (e,f) Mo 3d and S 2p spectrum's of MS-ZNO-5.

2.2. Gas Sensing Properties

In this portion, the gas sensing properties of various sensors were studied. Their deep explanation was as follows: the response/recovery time curves for MS-ZNO-0, MS-ZNO-5 and MS-ZNO-10 were depicted in Figure 5a, which showed that response/recovery times for 2 ppm H₂S were 10 s/6 s, (Figure 5b). Importantly, the minimum response of 1.8 to 0.05 ppm H₂S was detected. The modification of octahedron MoS₂ with ZnO-Zn₂SnO₄ nanoparticles not only enhances the BET surface area but also intensifies the adsorption of H₂S molecules on the surface of the material, and it may also facilitate the adsorption of the oxygen species. These can be some factors which increase the gas sensing properties of nanocomposite (MS-ZNO-5). In Table 1, the gas sensing properties of the current sensor and some previous sensors were studied, which stated that the sensor based on MS-ZNO-5 received lower temperature gas sensing, better response, humble selectivity, LOD and rapid response/recovery times. Figure 5c was the temperature–resistance diagram of MS-ZNO-0, MS-ZNO-5 and MS-ZNO-10 at the operating temperature of 30 °C in air. When the operating temperature increased, the resistance showed a downward trend; this is because, when heating, the O^{2−} on the surface of both materials adsorbed oxygen and O^{2−} was converted into O[−], which produces a large number of free electrons. At the same time, a large number of electrons reduced the concentration of negative ions on the surface of all the materials; in this way the potential barrier was twisted and the resistance was finally reduced [38,39]. As the temperature continued to enhance, the resistance of materials continued to decrease as the electrons moved faster. Figure 5d described the response vs. temperature curves, which specified that the response was improving with the increase in H₂S concentrations. Thus, due to the linearity of the current sensor, it could be considered a promising material because of the linear relationship between H₂S ppm and response. In Figure 5e, three sensors based on synthesized nanocomposites were tested to 2 ppm H₂S at different operating temperatures. The maximum response detected by the sensor of MS-ZNO-5 was 4 to 2 ppm H₂S at 30 °C. The decrease in response at higher temperatures could be explained as follows: the chemical activity is low at lower operating temperature, and vice versa. As a result, more gas molecules adsorbed onto the material surface quickly at higher temperatures, resulting in a decrease in response [40].

Figure 6a stated that the highest response to 2 ppm H₂S was 4 and the second highest response to 2 ppm TMA was 2.5 at the operating temperature of 30 °C; in this way, the humble selectivity ($S_{2\text{ ppm H}_2\text{S}}/S_{2\text{ ppm TMA}} = 1.6$) was detected. The results about the reproducibility in Figure 6b demonstrated that the sensor based on MS-ZNO-5 showed promising reproducibility; it was checked around five times at the operating temperature of 30 °C and a similar response was noted. While other sensors detected good reproducibility, our main concern was the gas sensing properties of MS-ZNO-5. For this reason, the promising reproducibility was studied in correspondence with the sensor of MS-ZNO-5. The improvement in gas sensing response corresponded to some aspects such as the octahedron structure of MoS₂; this enhanced BET surface area, allowing more oxygen species to adsorb onto the surface of the material and make the reaction faster to increase the gas sensing response [17].

The stability evaluation in Figure 7a explained that the sensors of MS-ZNO-0, MS-ZNO-5 and MS-ZNO-10 were almost stable for approximately 35 days. The resistance of all the sensors decreased slightly with time. To date, the majority of the gas sensors based on semiconductor gas sensors were not satisfied, which demerits their applications in the field of gas sensors. However, in the present case we may see that the long-term stability was quite stable for almost a month. Different responses (3.2, 4, 3.4, and 3.4) to 2 ppm H₂S were detected by the sensor of MS-ZNO-5 at various relative humidities (RH) of 20, 40, 60, and 80, respectively; the detail was revealed in Figure 7b. The highest response was detected at the 40% RH value. The results explained that the response was decreased after 40% RH due to the presence of the higher amount of water molecules with increased relative humidity; these can be adsorbed onto the surface of the material, and accordingly, the resistance decreases [41]. The results proved that the sensor based on MS-ZNO-5 was noteworthy in

all aspects such as high response, humble selectivity, rapid response–recovery times, LOD, good stability, an almost linear relation between H₂S gas concentration and response, etc.

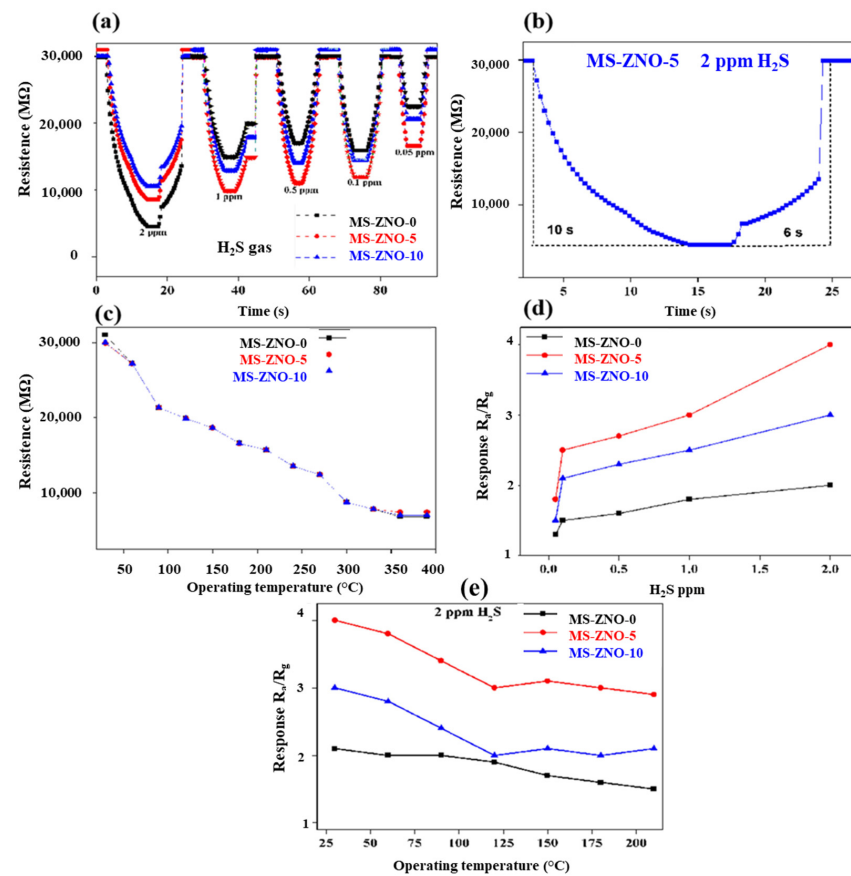


Figure 5. (a) Dynamic responses of all sensors to H₂S 0.05–2 ppm at the operating temperature of 30 °C; (b) response/recovery diagram of MS-ZNO-5 towards 2 ppm H₂S; (c) temperature resistance of pure and composite materials towards 2 ppm in the air at 30 °C; (d) graph of the relationship between the different concentration of H₂S ppm and response at 30 °C; (e) the responses of all sensors towards 2 ppm H₂S at various operating temperatures.

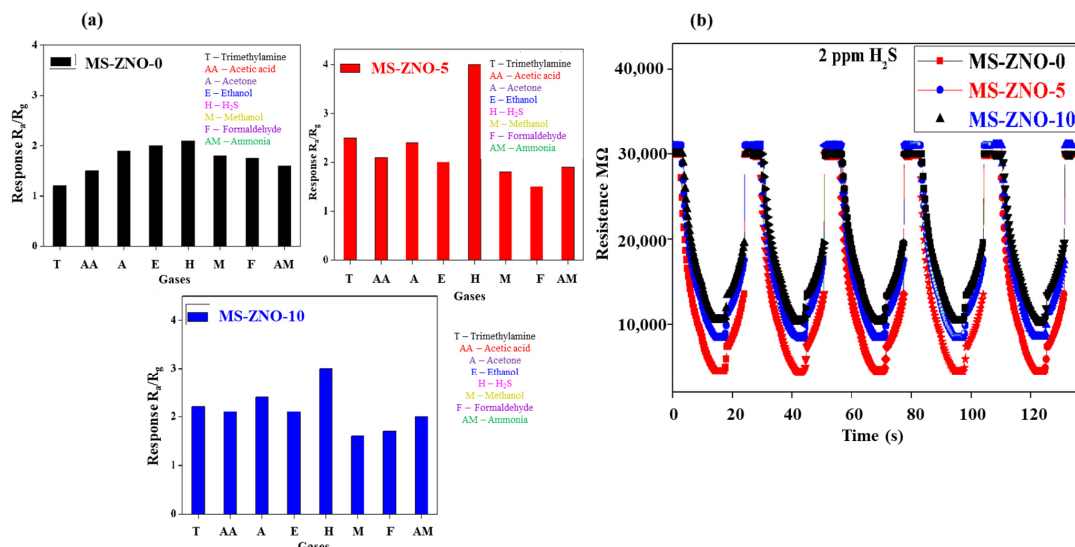


Figure 6. (a) Responses of MS-ZNO-0, MS-ZNO-5 and MS-ZNO-10 towards different gases (2 ppm); (b) reproducibility graphs of MS-ZNO-0, MS-ZNO-5 and MS-ZNO-10.

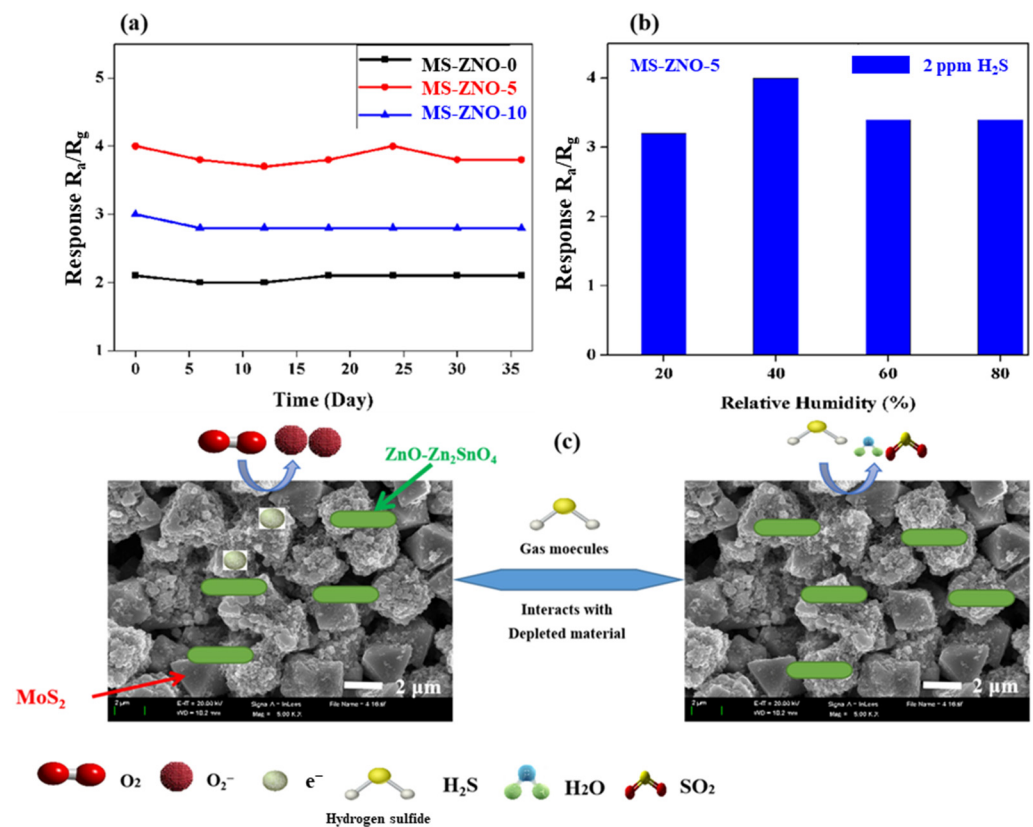
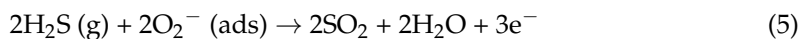


Figure 7. (a) The stability graph; (b) relationship between response of MS–ZNO–5 to 2 ppm H₂S and different relative humidity at 30 °C; (c) diagram of gas sensing mechanism.

2.3. Gas Sensing Mechanism

N-type gas sensing behavior was discussed based on the sensor of MS-ZNO-5 described in Figure 7c. Usually, all SMOs involve three steps, such as (1) adsorption; (2) oxidation; and (3) desorption. When the sensor of MS-ZNO-5 was tested in the air ambience, the process was similar to our previous work [10]; first, oxygen molecules were adsorbed onto the surface of the material. There, they converted the captured electrons from the conduction band of ZnO-Zn₂SnO₄ into oxygen ions such as O⁻, O²⁻, and O₂⁻, while forming the electron depletion layer and enhancing the sensor resistance, which was described in Equations (1)–(4). The adsorbed oxygen species depends on the operating temperatures, as shown in the following equations [42]. When the sensor of MS-ZNO-5 was tested in gas ambience, the molecules of H₂S reacted with oxygen ions and converted them into H₂O and SO₂, as mentioned in Equation (5). After that, the captured electrons were discharged back, due to the decrease in the resistance and space charge layer [10]. Thus, the sensor of MS-ZNO-5 showed a low resistance in gas atmosphere [43,44]. Further detail about the sensing mechanism has been given in the Equations below.





Enhancement in gas sensing response of MS-ZNO-5 may correspond to some parameters due to the attachment of octahedron MoS₂. Firstly, the formation of the n-n junction can also be one of the factors used to enhance gas sensing properties; the octahedron structure of MoS₂ was checked by SEM and TEM [45]; the octahedron structure developed the exposure of active edge sites of MoS₂, and improved the efficiency of gas transportation, reaction and carrier exchange, etc. This resulted in the enhanced H₂S gas sensing properties and increased BET-specific surface area of MS-ZNO-5 (N₂ adsorption–desorption isotherms); this factor can be very helpful to the adsorption and diffusion of H₂S molecules. Moreover, the attachment with octahedron MoS₂ increased the conductivity of the noteworthy composite [45] and enlarged the number of oxygen species (XPS), etc. This was also one of the parameters used to enhance their performance.

Table 1. The comparison of sensing properties between some sensors.

Materials	Temp. (°C)	Gas/Conc. ppm	Response (R _g /R _a)	Selectivity	Limit of Detection	Ref.
ZnSnO ₃	230	ethanol/50	47	1.4	1 ppm	[46]
ZnO/Co ₃ O ₄	250	acetone/50	46	-	2 ppm	[47]
ZnO-ZnS	150	H ₂ S/5	0.88	-	1 ppm	[48]
Pd/ZnO	220	CO/100	15	-	20 ppm	[49]
Zn ₂ SnO ₄	133	H ₂ S/1	-	-	1 ppb	[50]
Nb ₂ O ₅ /SnO ₂	275	H ₂ S/20	4	3.8	-	[51]
Ag-In ₂ O ₃	30	H ₂ S/20	93719	-	0.005 ppm	[52]
MoS ₂ -ZnO-Zn ₂ SnO ₄	30	H ₂ S/2	4	1.6	0.05 ppm	This work

Temp. = temperature, Conc. = concentration, Ref. = reference.

3. Experimental Section

3.1. Chemicals

The chemicals (molybdenum disulfide (MoS₂), zinc nitrate hexahydrate (Zn(NO₃)₂·6H₂O), tin chloride pentahydrate (SnCl₄·5H₂O) and sodium hydroxide (NaOH)) utilized in the synthesis method of ZnO-Zn₂SnO₄ nanoparticles and MoS₂-ZnO-Zn₂SnO₄ nanocomposites were bought from the Sinopharm Chemical Reagent Limited Corporation (Dalian, China) and all these chemicals were used without further purification.

3.2. The Synthesis of ZnO-Zn₂SnO₄ Nanoparticles and MoS₂-ZnO-Zn₂SnO₄ Nanocomposite

Hydrothermal was used to synthesize ZnO-Zn₂SnO₄ nanoparticles and MoS₂-ZnO-Zn₂SnO₄ nanocomposites. Concisely, Zn(NO₃)₂·6H₂O (8 mmol, 1.477 g), and SnCl₄·5H₂O (4 mmol, 0.876 g) were mixed into three different beakers (1, 2 and 3) with 50 mL deionized water while stirring and then different contents of MoS₂, such as 0 wt% MoS₂ (MS-ZNO-0), 5 wt% MoS₂ (MS-ZNO-5) and 10 wt% MoS₂ (MS-ZNO-10), were added into beaker numbers 1, 2 and 3, respectively. After half an hour, 2M NaOH solution was gradually added to all the beakers to adjust the pH to about 12. The stirring process was carried out for 24 h to thoroughly mix all the ingredients and to receive the milky solutions. Furthermore, there was an autoclave process in which the samples were transferred into 100 mL stainless steel autoclaves and placed into an oven, and the time (20 h) and temperature (190 °C) were adjusted. After the autoclave process, the powder materials were separated by centrifugation process (washing with ethanol and DI water, 8000 rpm) and drying process (heating 60 °C, 20 h). Finally, the white products were calcined at 300 °C, 3 h and 5 °C/min. After that, the fabrication of gas sensors for gas sensing performances and other characteristics was carried out to check crystallite size, morphology and other properties of all the samples. The dried samples after calcination were ground in a mortar for fabricating the sensors and also for other characterizations such as XRD, SEM, TEM, etc.

3.3. Characterizations of the Nanocomposites

Numerous characterizations have been used to identify the crystal size, BET-specific surface area, morphology and surface properties of synthesized products. Their deep explanation has been studied as follows: X-ray diffraction (XRD, D/MAX-Ultima, Cu K α source, 2°/min scanning rate, scanning angle from 10°–80° as well as power of 40 kV and 40 mA, Rigaku, Tokyo, Japan), BET method (ASAP2010C instrument, Norcross, GA, USA), scanning electron microscopy (SEM, Suppa 55 Sapphire, Carl Zeiss AG, Jena, Germany), transmission electron microscopy (TEM, JEM-3200FS, JEOL, Tokyo, Japan), energy-dispersive X-ray spectroscopy (EDS, Sapphire 55 Supra, Zeiss, Jena, Germany) and X-ray photoelectron spectroscopy (XPS, Thermo Scientific ESCALAB 250 XI, ThermoFisher Scientific, Waltham, MA, USA) were used to check the crystal size, BET-specific surface area, morphology and surface properties of synthesized products. These tests were best performed by providing powder samples for XRD (about 20–30 mg of powder), SEM (about 10 mg of powder), TEM (about 10 mg of powder), EDS (about 10 mg of powder), BET (about 200 mg of powder) and XPS (about 5–10 mg of powder), respectively.

3.4. Fabrication of Gas Sensor

The gas sensor diagram and the electrical circuit were displayed in Figure 8. The fabrication process of the gas sensor was studied as follows: firstly, the paste was made with 0.2 g nanocomposite and 2–3 drops of terpeneol and then the mixture was coated onto the outer surface of the alumina tube. After that, the alumina tube was heated in an oven for 10 h at 80 °C to remove the contents of terpeneol. Then, a Ni-Cr alloy wire was placed in the alumina tube to control the operating temperature in the range of 30–400 °C. All the hazardous gases detected in the present work were bought from the Dalian Haide Technology Company Limited (Dalian China). The gas sensor based on MoS₂-ZnO-Zn₂SnO₄ nanocomposites showed n-type gas sensor behavior and the response was calculated as $S = R_a/R_g$, where R_a was the resistance in air and R_g was the resistance in the gas. The selectivity of the sensor was calculated in this study, which may be defined as the ratio of the highest response and second highest response; in the present case, it was ' $S_{10\text{ppm H}_2\text{S}}/S_{10\text{ppm TMA}} = 1.6'$ ', and likewise response/recovery times were stated as the time taken to reach 90% value of the final signal. The sensors were stable for 35 days and reproducible for five cycles.

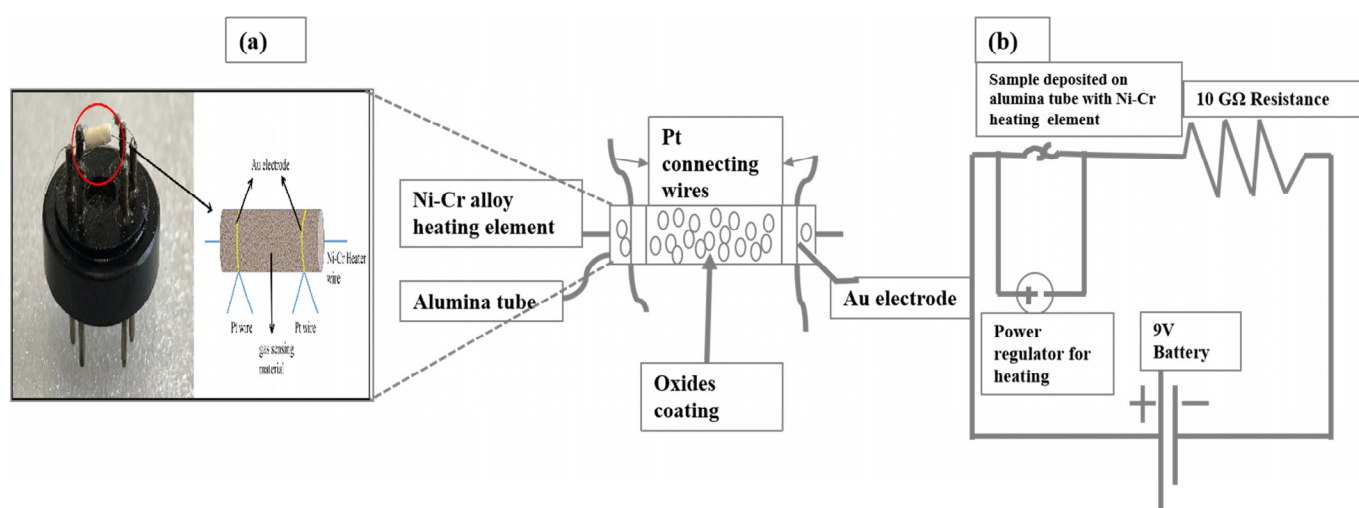


Figure 8. (a) The gas sensor device diagram and (b) the electrical circuit [8].

4. Conclusions

The pure ZnO-Zn₂SnO₄ nanoparticles and nanocomposites were synthesized via a hydrothermal method. The synthesized materials were characterized using XRD, BET method, SEM, TEM, EDS and XPS, respectively. The XRD and SEM results may relate to

each other, and we studied to see why the crystallite size and particle were increased when ZnO-Zn₂SnO₄ nanoparticles were attached with octahedron MoS₂, respectively. From BET and XPS results, it was concluded that the MS-ZNO-5 nanocomposite revealed higher BET-specific surface area and more adsorption of oxygen species than MS-ZNO-0, which could be the main factors enhancing the gas sensing properties. The gas sensing properties of three gas sensors based on MS-ZNO-0, MS-ZNO-5 and MS-ZNO-10 were studied. The gas sensor based on an MS-ZNO-5 nanocomposite detected the highest response to 2 ppm H₂S, and humble selectivity, rapid response/recovery time, good stability, promising reproducibility and LOD (0.05 ppm) were noticed. Furthermore, the sensor of MS-ZNO-0 and MS-ZNO-10 detected far fewer responses towards all gases. The enhancement in gas sensing response of MS-ZNO-5 corresponded with some parameters such as layered structure, n-n junction, higher BET surface area, more adsorption of oxygen species, etc. An almost linear relation between response and concentration of H₂S (0.05–2 ppm) could allow the current sensor to be considered a potential candidate for gas sensing applications in the detection of and warning about leakage of hazardous VOCs.

Author Contributions: Conceptualization, D.W. and A.A.; methodology, A.A.; validation, A.A.; investigation, D.W. and A.A.; resources, A.A.; writing—original draft preparation, D.W. and A.A.; writing—review and editing, D.W. and A.A.; supervision, A.A. All authors have read and agreed to the published version of the manuscript.

Funding: This work is financially supported by the Scientific Research Funding Project of Educational Department of Liaoning Province (Grant No. LJKZ0060), the Liaoning Applied Fundamental Research Project (Grant No. 2022JH2/101300158).

Institutional Review Board Statement: Not applicable.

Informed Consent Statement: Not applicable.

Data Availability Statement: The data can be provided on the responsible request to the corresponding author.

Conflicts of Interest: The authors declare no conflict of interest.

Sample Availability: Samples of the compounds are available from the authors.

References

1. Tong, X.; Shen, W.; Chen, X.; Corriou, J.P. A fast response and recovery H₂S gas sensor based on free-standing TiO₂ nanotube array films prepared by one-step anodization method. *Ceram. Int.* **2017**, *43*, 14200–14209. [[CrossRef](#)]
2. Han, C.; Li, X.; Shah, C.; Li, X.; Ma, J.; Zhang, X.; Liu, Y. Composition-controllable p-CuO/n-ZnO hollow nanofibers for high-performance H₂S detection. *Sens. Actuators B Chem.* **2019**, *285*, 495–503. [[CrossRef](#)]
3. Samokhvalov, A.; Tatarchuk, B.J. Characterization of active sites, determination of mechanisms of H₂S, COS and CS₂ sorption and regeneration of ZnO low-temperature sorbents: Past, current and perspectives. *Phys. Chem. Chem. Phys.* **2011**, *13*, 3197–3209. [[CrossRef](#)] [[PubMed](#)]
4. Hsueh, T.J.; Ding, R.Y. A Room Temperature ZnO-NPs/MEMS Ammonia Gas Sensor. *Nanomaterials* **2022**, *12*, 3287. [[CrossRef](#)] [[PubMed](#)]
5. Ren, X.; Xu, Z.; Zhang, Z.; Tang, Z. Enhanced NO₂ Sensing Performance of ZnO-SnO₂ Heterojunction Derived from Metal-Organic Frameworks. *Nanomaterials* **2022**, *12*, 3726. [[CrossRef](#)]
6. Horng, R.H.; Lin, S.H.; Hung, D.R.; Chao, P.H.; Fu, P.K.; Chen, C.H.; Chen, Y.C.; Shah, J.H.; Huang, C.Y.; Tarntair, F.G.; et al. Structure Effect on the Response of ZnGa₂O₄ Gas Sensor for Nitric Oxide Applications. *Nanomaterials* **2022**, *12*, 3759. [[CrossRef](#)]
7. Yang, Y.; Maeng, B.; Jung, D.G.; Lee, J.; Kim, Y.; Kwon, J.; An, H.K.; Jung, D. Annealing Effects on SnO₂ Thin Film for H₂ Gas Sensing. *Nanomaterials* **2022**, *12*, 3227. [[CrossRef](#)] [[PubMed](#)]
8. Akhtar, A.; Sadaf, S.; Liu, J.; Wang, Y.; Wei, H.; Zhang, Q.; Fu, C.; Wang, J. Hydro-thermally synthesized spherical g-C₃N₄-NiCo₂O₄ nanocomposites for ppb level ethanol detection. *J. Alloy. Compd.* **2022**, *911*, 165048. [[CrossRef](#)]
9. Akhtar, A.; Jiao, C.; Chu, X.F.; Liang, S.; Dong, Y.; He, L. Acetone sensing properties of the g-C₃N₄-CuO nanocomposites prepared by hydrothermal method. *Mater. Chem. Phys.* **2021**, *265*, 124375. [[CrossRef](#)]
10. Akhtar, A.; Wen, H.; Chu, X.F.; Liang, S.; Dong, Y.; He, L.; Zhang, K. Synthesis of g-C₃N₄-Zn₂SnO₄ nanocomposites with enhanced sensing performance to ethanol vapor. *Synth. Met.* **2021**, *278*, 116829. [[CrossRef](#)]
11. Yan, T.; Liu, H.; Sun, M.; Wang, X.; Li, M.; Yan, Q.; Xu, W.; Du, B. Efficient photocatalytic degradation of bisphenol A and dye pollutants over BiOI/Zn₂SnO₄ hetero-junction photocatalyst. *RSC Adv.* **2015**, *5*, 10688–10696. [[CrossRef](#)]

12. Wang, K.; Shi, Y.; Guo, W.; Yu, X.; Ma, T. Zn₂SnO₄-Based Dye-Sensitized Solar Cells: Insight into Dye-Selectivity and Photoelectric Behaviors. *Electrochim. Acta* **2014**, *135*, 242–248. [[CrossRef](#)]
13. Shu, S.; Wang, M.; Yang, W.; Liu, S. Synthesis of surface layered hierarchical octahedron-like structured Zn₂SnO₄/SnO₂ with excellent sensing properties toward HCHO. *Sens. Actuators B Chem.* **2017**, *243*, 1171–1180. [[CrossRef](#)]
14. An, D.; Mao, N.; Deng, G.; Zou, Y.; Li, Y.; Wei, T.; Lian, X. Ethanol gas-sensing characteristic of the Zn₂SnO₄ nanospheres. *Ceram. Int.* **2016**, *42*, 3535–3541. [[CrossRef](#)]
15. Cao, F.F.; Li, C.P.; Li, M.J.; Li, H.J.; Huang, X.; Yang, B.H. Direct growth of Al-doped ZnO ultrathin nanosheets on electrode for ethanol gas sensor application. *Appl. Surf. Sci.* **2018**, *447*, 173–181. [[CrossRef](#)]
16. Zhang, Y.; Xin, X.; Sun, H.; Liu, Q.; Zhang, J.; Li, G.; Gao, J.; Lu, H.; Wang, C. Porous ZnO–SnO₂–Zn₂SnO₄ heterojunction nanofibers fabricated by electrospinning for enhanced ethanol sensing properties under UV irradiation. *J. Alloy. Compd.* **2021**, *854*, 157311. [[CrossRef](#)]
17. Hanha, N.H.; Duy, L.V.; Hung, C.M.; Xuan, C.T.; Duy, N.V.; Hoa, N.D. High-performance acetone gas sensor based on Pt–Zn₂SnO₄ hollow octahedra for diabetic diagnosis. *J. Alloy. Compd.* **2021**, *886*, 161284. [[CrossRef](#)]
18. Wang, B.; Zheng, Z.Q.; Zhu, L.F.; Yang, Y.H.; Wu, H.Y. Self-assembled and Pd decorated Zn₂SnO₄/ZnO wire-sheet shape nano-heterostructures networks hydrogen gas sensors. *Sens. Actuators B Chem.* **2014**, *195*, 549–561. [[CrossRef](#)]
19. Munusami, V.; Arutselvan, K.; Vadivel, S.; Govindasamy, S. High sensitivity LPG and H₂ gas sensing behavior of MoS₂/graphene hybrid sensors prepared by facile hydrothermal method. *Ceram. Int.* **2022**, *48*, 29322–29331. [[CrossRef](#)]
20. Ou, J.Z.; Ge, W.; Carey, B.; Daeneke, T.; Rotbart, A.; Shan, W.; Wang, Y.; Fu, Z.; Chrimes, A.F.; Wlodarski, W.; et al. Physisorption-Based Charge Transfer in Two-Dimensional SnS₂ for Selective and Reversible NO₂ Gas Sensing. *ACS Nano* **2015**, *9*, 10313–10323. [[CrossRef](#)]
21. Zhou, H.; Xu, K.; Ha, N.; Cheng, Y.; Ou, R.; Ma, Q.; Hu, Y.; Trinh, V.; Ren, G.; Li, Z.; et al. Reversible Room Temperature H₂ Gas Sensing Based on Self-Assembled Cobalt Oxysulfide. *Sensors* **2022**, *22*, 303. [[CrossRef](#)] [[PubMed](#)]
22. Cheng, Y.; Ren, B.; Xu, K.; Jeerapan, I.; Chen, H.; Li, Z.; Ou, J.Z. Recent progress in intrinsic and stimulated room-temperature gas sensors enabled by low-dimensional materials. *J. Mater. Chem. C* **2021**, *9*, 3026–3051. [[CrossRef](#)]
23. Xu, K.; Ha, N.; Hu, Y.; Ma, Q.; Chen, W.; Wen, X.; Ou, R.; Trinh, V.; McConville, C.F.; Zhang, B.Y.; et al. A room temperature all-optical sensor based on two-dimensional SnS₂ for highly sensitive and reversible NO₂ sensing. *J. Hazard. Mater.* **2022**, *426*, 127813. [[CrossRef](#)]
24. Alkathiri, T.; Xu, K.; Zhang, B.Y.; Khan, M.Y.; Jannat, A.; Syed, N.; Almutairi, A.F.M.; Ha, N.; Alsaif, M.M.Y.A.; Pillai, N.; et al. 2D Palladium Sulphate for Visible-Light-Driven Optoelectronic Reversible Gas Sensing at Room Temperature. *Small Sci.* **2022**, *2*, 2100097. [[CrossRef](#)]
25. Li, K.; Du, C.; Gao, H.; Yin, T.; Yu, Y.; Wang, W. Ultra-fast and linear polarization-sensitive photodetectors based on ReSe₂/MoS₂ van der Waals heterostructures. *J. Mater.* **2022**, *8*, 1158–1164. [[CrossRef](#)]
26. Abdelazeez, A.A.A.; Trabelsi, A.B.G.; Alkallas, F.H.; Rabia, M. Successful 2D MoS₂ nanosheets synthesis with SnSe grid-like nanoparticles: Photoelectrochemical hydrogen generation and solar cell applications. *Sol. Energy* **2022**, *248*, 251–259. [[CrossRef](#)]
27. Zhao, W.; Yan, R.; Li, H.; Ding, K.; Chen, Y.; Xu, D. Highly sensitive NO₂ gas sensor with a low detection limit based on Pt-modified MoS₂ flakes. *Mater. Lett.* **2023**, *330*, 133386. [[CrossRef](#)]
28. Li, W.; Li, H.; Qian, R.; Zhuo, S.; Ju, P.; Chen, Q. CTAB Enhanced Room-Temperature Detection of NO₂ Based on MoS₂-Reduced Graphene Oxide Nanohybrid. *Nanomaterials* **2022**, *12*, 1300. [[CrossRef](#)]
29. Li, W.; Shahbazi, M.; Xing, K.; Tesfamichael, T.; Motta, N.; Qi, D.C. Highly Sensitive NO₂ Gas Sensors Based on MoS₂@MoO₃ Magnetic Heterostructure. *Nanomaterials* **2022**, *12*, 1303. [[CrossRef](#)]
30. Xia, Y.; Wu, Z.; Qin, Z.; Chen, F.; Lv, C.; Zhang, M.; Shaymurat, T.; Duan, H. Wool-Based Carbon Fiber/MoS₂ Composite Prepared by Low-Temperature Catalytic Hydrothermal Method and Its Application in the Field of Gas Sensors. *Nanomaterials* **2022**, *12*, 1105. [[CrossRef](#)]
31. Wang, S.; Chen, W.; Li, J.; Song, Z.; Zhang, H.; Zeng, W. Low Working Temperature of ZnO–MoS₂ Nanocomposites for Delaying Aging with Good Acetylene Gas-Sensing Properties. *Nanomaterials* **2020**, *10*, 1902. [[CrossRef](#)]
32. Parthibavarman, M.; Vallalperuman, K.; Sathishkumar, S.; Durairaj, M.; Thavamani, K. A novel microwave synthesis of nanocrystalline SnO₂ and its structural optical and dielectric properties. *J. Mater. Sci. Mater. Electron.* **2014**, *25*, 730–735. [[CrossRef](#)]
33. Zhang, C.; Shao, X.; Li, C.; Wang, M.; Zhang, M.; Liu, Y. Electrospun nanofibers of p type NiO/n-type ZnO heterojunctions with enhanced photocatalytic activity. *ACS Appl. Mater. Interfaces* **2010**, *2*, 2915–2923. [[CrossRef](#)]
34. Han, L.; Liu, J.; Wang, Z.; Zhang, K.; Luo, H.; Xu, B.; Zou, X.; Zheng, X.; Ye, B.; Yu, X. Shape-controlled synthesis of ZnSn(OH)₆ crystallites and their HCHO-sensing properties. *CrystrEngComm* **2012**, *14*, 3380–3386. [[CrossRef](#)]
35. Chang, X.; Qiao, X.; Li, K.; Wang, P.; Xiong, Y.; Li, X.; Xia, F.; Xue, Q. UV assisted ppb level acetone detection based on hollow ZnO/MoS₂ nanosheets core/shell heterostructures at low temperature. *Sens. Actuators B Chem.* **2020**, *317*, 128208. [[CrossRef](#)]
36. Chakraborty, A.; Kebede, M. Preparation and characterization of WO₃/Bi₃O₄Cl nanocomposite and its photocatalytic behavior under visible light irradiation. *React. Kinet. Mech. Catal.* **2012**, *106*, 83–98. [[CrossRef](#)]
37. Lei, Y.; Guo, P.; Jia, M.; Wang, W.; Liu, J.; Zhai, J. One-step photo-deposition synthesis of TiO₂ nanobelts/MoS₂ quantum dots/rGO ternary composite with remarkably enhanced photocatalytic activity. *J. Mater. Sci.* **2020**, *55*, 14773–14786. [[CrossRef](#)]
38. Liu, X.; Cheng, B.; Jifan, H.; Qin, H.; Jiang, M. Preparation, structure, resistance and methane-gas sensing properties of nominal La_{1-x}Mg_xFeO₃. *Sens. Actuators B Chem.* **2008**, *133*, 340–344. [[CrossRef](#)]

39. Li, X.; Zhang, Y.; Bhattacharya, A.; Chu, X.; Liang, S.; Zeng, D. The formaldehyde sensing properties of CdGa₂O₄ prepared by co-precipitation method. *Sens. Actuators B Chem.* **2021**, *343*, 129834. [[CrossRef](#)]
40. Liu, L.; Li, S.C.; Zhuang, J.; Wang, L.Y.; Zhang, J.B.; Li, H.Y.; Liu, Z.; Han, Y.; Jiang, X.X.; Zhang, P. Improved selective acetone sensing properties of Co-doped ZnO nanofibers by electrospinning. *Sens. Actuator B Chem.* **2011**, *155*, 782–788. [[CrossRef](#)]
41. Xu, J.Q.; Xue, Z.G.; Qin, N.; Cheng, Z.X.; Xiang, Q. The crystal facet-dependent gas sensing properties of ZnO nanosheets: Experimental and computational study. *Sens. Actuator B-Chem.* **2017**, *242*, 148–157. [[CrossRef](#)]
42. Li, Q.; Chen, D.; Miao, J.; Lin, S.; Yu, Z.; Han, Y.; Yang, Z.; Zhi, X.; Cui, D.; An, Z. Ag-modified 3D reduced graphene oxide aerogel-based sensor with an embedded microheater for a fast response and high-sensitive detection of NO₂. *ACS Appl. Mater. Interfaces* **2020**, *12*, 25243–25252. [[CrossRef](#)]
43. Chen, Y.J.; Yu, L.; Feng, D.D.; Zhuo, M.; Zhang, M.; Zhang, E.D.; Xu, Z.; Li, Q.H.; Wang, T.H. Superior ethanol-sensing properties based on Ni-doped SnO₂ p–n hetero-junction hollow spheres. *Sens. Actuators B Chem.* **2012**, *166–167*, 61–67. [[CrossRef](#)]
44. Wang, X.; Liu, F.; Xie, X.; Xu, G.; Tian, J.; Cui, H. Au modified single crystalline and polycrystalline composite tin oxide for enhanced n-butanol sensing performance. *Powder Technol.* **2018**, *331*, 270–275. [[CrossRef](#)]
45. Li, Y.; Song, Z.; Li, Y.; Chen, S.; Li, S.; Li, Y.; Wang, H.; Wang, Z. Hierarchical hollow MoS₂ microspheres as materials for conductometric NO₂ gas sensors. *Sens. Actuators B Chem.* **2019**, *282*, 259–267. [[CrossRef](#)]
46. Zhang, D.; Zhang, Y.; Fan, Y.; Luo, N.; Cheng, Z.; Xu, J. Micro-spherical ZnSnO₃ material prepared by microwave-assisted method and its ethanol sensing properties. *Chin. Chem. Lett.* **2020**, *31*, 2087–2090. [[CrossRef](#)]
47. Lei, M.; Zhou, X.; Zou, Y.; Ma, J.; Alharthi, F.A.; Alghamdi, A.; Yang, X.; Deng, Y. A facile construction of heterostructured ZnO/Co₃O₄ mesoporous spheres and superior acetone sensing performance. *Chin. Chem. Lett.* **2021**, *32*, 1998–2004. [[CrossRef](#)]
48. Ding, P.; Xu, D.; Dong, N.; Chen, Y.; Xu, P.; Zheng, D.; Li, X. A high-sensitivity H₂S gas sensor based on optimized ZnO-ZnS nano-heterojunction sensing material. *Chin. Chem. Lett.* **2020**, *31*, 2050–2054. [[CrossRef](#)]
49. Luo, N.; Zhang, B.; Zhang, D.; Xu, J. Enhanced CO sensing properties of Pd modified ZnO porous nanosheets. *Chin. Chem. Lett.* **2020**, *31*, 2033–2036. [[CrossRef](#)]
50. Xu, T.T.; Zhang, X.F.; Dong, X.; Deng, Z.P.; Huo, L.H.; Gao, S. Enhanced H₂S gas-sensing performance of Zn₂SnO₄ hierarchical quasi-microspheres constructed from nanosheets and octahedra. *J. Hazard. Mater.* **2019**, *361*, B49–B55. [[CrossRef](#)]
51. Mao, L.W.; Zhu, L.Y.; Wu, T.T.; Xu, L.; Jin, X.H.; Lu, H.L. Excellent long-term stable H₂S gas sensor based on Nb₂O₅/SnO₂ core-shell heterostructure nanorods. *Appl. Surf. Sci.* **2022**, *602*, 154339. [[CrossRef](#)]
52. Yan, S.; Li, Z.; Li, H.; Wu, Z.; Wang, J.; Shen, W.; Fu, Y.Q. Ultra-sensitive room-temperature H₂S sensor using Ag–In₂O₃ nanorod composites. *J. Mater. Sci.* **2018**, *53*, 16331–16344. [[CrossRef](#)]

Disclaimer/Publisher’s Note: The statements, opinions and data contained in all publications are solely those of the individual author(s) and contributor(s) and not of MDPI and/or the editor(s). MDPI and/or the editor(s) disclaim responsibility for any injury to people or property resulting from any ideas, methods, instructions or products referred to in the content.